Center for Turbulence Research
Proceedings of the Summer Program 2008

A comparison of various equal-order interpolation methodologies using the method of manufactured solutions

By S. P. Domino†

This paper represents a first step to providing a comparison between a suite of approximate projection methods and stabilized equal-order, i.e., the primitive variables are collocated with an equal-order interpolation basis, fully coupled methods. The paper first reviews splitting and stabilization errors that appear in many common approximate projection methods. The approximate pressure projection analysis demonstates a conflicted role for the pressure stabilization scaling parameter. This parameter must be chosen to control both splitting errors and stabilization errors. However, for fully coupled schemes splitting errors are not of consequence. Therefore, a stabilization parameter can be chosen to most appropriately control stabilization errors. A fully coupled equal-order scheme is proposed with two forms of the stabilization parameter. A set of manufactured solutions are run to verify the accuracy of this new method.

1. Introduction

In the previous Center for Turbulence Research Summer Program, the role of explicit stabilization in the context of common equal-order pressure projection schemes was outlined (Domino 2006). A family of projection methods was defined based on various time scale choices. Three common approximate projection methods were presented in detail. A formal manufactured solution was presented to verify that the standard time step stabilization parameter leads to first-order time accuracy despite the underlying second-order time integration scheme.

To review, the analysis of a given computational fluids algorithm begins with the discrete momentum and continuity equations written in matrix form. The matrix $\mathbf{A}$ contains discrete, linearized contributions to the momentum equations from the time derivative, convection and diffusion terms,

$$\begin{bmatrix} \mathbf{A} & \mathbf{G} \\ \mathbf{D} & \mathbf{0} \end{bmatrix} \begin{bmatrix} \mathbf{u}^{n+1} \\ p^{n+1/2} \end{bmatrix} = \begin{bmatrix} \mathbf{f} \\ \mathbf{b} \end{bmatrix}. \tag{1.1}$$

The discrete nodal gradient and nodal divergence are $\mathbf{G}$ and $\mathbf{D}$, respectively. The function $\mathbf{f}$ contains the additional terms for the momentum equations, e.g., body force terms, while the function $\mathbf{b}$ can contain the appropriate terms for a non-solenoidal velocity field, i.e., $-\int \frac{\partial \rho}{\partial t} dV$. Finally, variable density aspects can be provided in the exact form of $\mathbf{D}$.

As previously described in Domino (2006) the full set of splitting and stabilization errors in the context of a fourth-order stabilized general approximate projection method are given by:

† Computational Thermal and Fluid Mechanics, Sandia National Laboratories

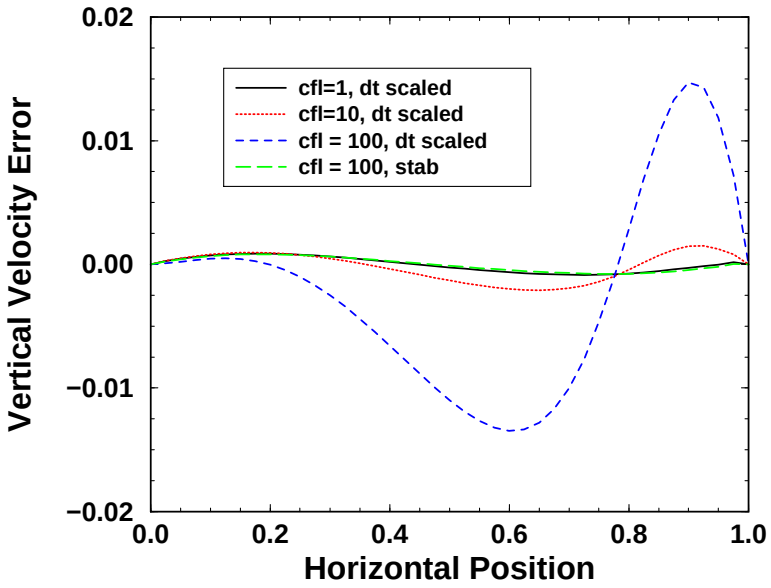

FIGURE 1. Plot of error profiles for the y-component of velocity for a driven cavity (see Ghia *et al.* 1983) flow using various time step scaling parameters. Also shown is the *stabilized* method described in Domino (2006) that uses a combination of time step and characteristic scaling.

$$\begin{bmatrix} \mathbf{A} & \mathbf{G} \\ \mathbf{D} & \mathbf{0} \end{bmatrix} \begin{bmatrix} \mathbf{u}^{n+1} \\ p^{n+1/2} \end{bmatrix} = \begin{bmatrix} \mathbf{f} \\ \mathbf{b} \end{bmatrix} + \begin{bmatrix} (\mathbf{I} - \mathbf{A}\tilde{\tau})\mathbf{G}(p^{n+\frac{1}{2}} - p^{n-\frac{1}{2}}) \\ (\mathbf{L}_\tau - \mathbf{D}\tilde{\tau}\mathbf{G})p^{n+\frac{1}{2}} \end{bmatrix}. \tag{1.2}$$

The error appearing in the momentum equation is due to splitting the original fully coupled system, Eq. (1.1), followed by a projection step. For a transient problem, which is the general interest to this project, the optimal $\tilde{\tau}$ approximates the diagonal of $\mathbf{A}$ which scales as Δt. This scaling is termed *time step scaling*. However, this choice of stabilization parameter leads to a time error that is first order accurate for practical pressure fields as $(\mathbf{L}_\tau - \mathbf{D}\tilde{\tau}\mathbf{G})p^{n+\frac{1}{2}}$ does not vanish, (Domino (2006)). Moreover, and perhaps as troubling, if a psuedo-transient algorithm is used to provide a steady state result, the results are a function of the time step taken (see, for example, Fig. 1).

Conversely, the optimal $\tilde{\tau}$ from the perspective of controlling stabilization errors scales as a linear combination of convection and diffusion time scales that represent the steady terms that appear in $\mathbf{A}$. However, the use of the *characteristic scaling* results in a particularly poor approximation to $\mathbf{A}^{-1}$ when any transient solution procedure is used. In such algorithms, in fact, stability issues are noted. Figure 2 represents the non-linear convergence within a time step for a transient, variable density, turbulent (using the standard two-equation k-ϵ model) buoyant Helium plume using two stabilization scalings. In this example, as is noted for most all transient flows, the characteristic scaling (regardless of linearizations) fails to converge within a time step. However, when the same simulation is run to converge the steady solution, even in the context of a psuedo-transient flow algorithm, a reasonable non-linear convergence behavior is obtained (see Fig. 3), although removal of low frequency error is slow.

Finally, it is emphasized that for approximate projection methods, $\mathbf{L_2} \neq \mathbf{D}\tilde{\tau}_2\mathbf{G}$ (cf. Almgren *et al.* 2000, Codina & Badia 2005).

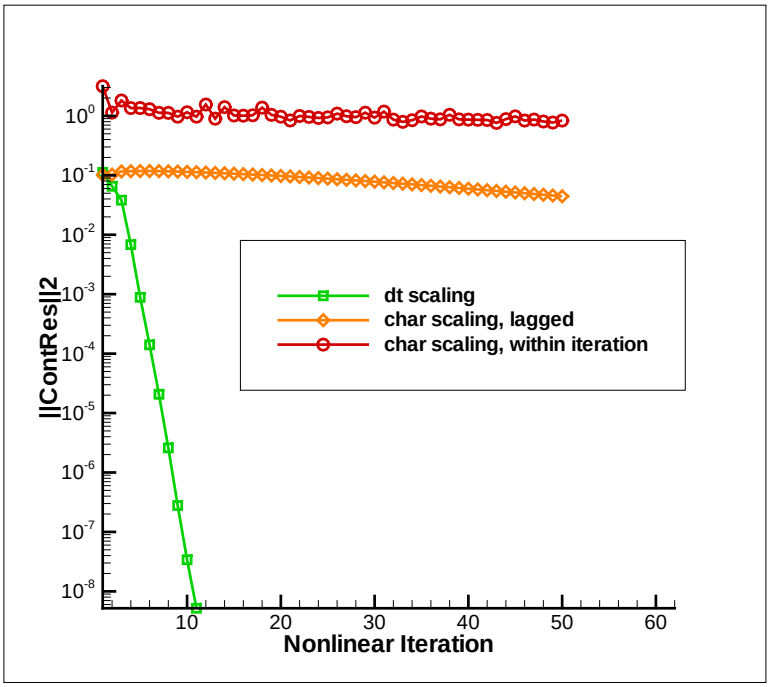

FIGURE 2. Plot of non-linear error norms within a given time step as a function of non-linear iteration comparing time step and characteristic scaling. Also shown is the effect of lagging the characteristic scaling parameter.

The above formal analysis, along with common simulation examples, suggests an inherent conflict of a single stabilization parameter to control *both* stabilization *and* splitting errors. The goal of this study is to provide an alternative to the segregated scheme by introducing a fully coupled equal-order pressure stabilized scheme that is given by,

$$\begin{bmatrix} \mathbf{A} & \mathbf{G} \\ \mathbf{D} & -\mathbf{L}_\tau \end{bmatrix} \begin{bmatrix} \mathbf{u}^{n+1} \\ p^{n+1/2} \end{bmatrix} = \begin{bmatrix} \mathbf{f} \\ -\int \frac{\partial \rho}{\partial t} dV - \alpha \mathbf{D} \tau \mathbf{G} \mathbf{p}^{\mathbf{n-1/2}} \end{bmatrix}. \tag{1.3}$$

The above system is proposed to be solved in a fully coupled manner so that the role of splitting error is removed and, therefore, will not effect the stability of the scheme. The above factor α determines the stabilzation order, i.e., $\alpha = 1$ provides a standard fourth-order stabilization as the full stabilization operator is a linear combination of the discrete Laplace operator and the blended nodal gradient. A value of α equal to zero provides a classic second-order stabilization afforded by the standard Laplace operator.

It is evident from the above system, Eq. (1.3), that the stabilization error remains as is shown in Eq. (1.2), however, it is now noted that the stabilization paramter can be determined solely from a criteria to control stabilization error in an optimal manner. In practice, it may still be advantagous to choose $\tilde{\tau}$ as strictly proportional to Δt. Note that this proposed scheme is not a so-called residual-based stabilization scheme (cf. Bochev *et al.* 2007) and does not suffer the standard stability limits from an arbitrarily small time step choice as the resulting pressure stabilized matrix operator is not *coercive*.

In practice, the stabilization parameter $\tilde{\tau}$ can be chosen such that it is a blend between a convection and diffusion time scale that will scale as Δx^2 thereby providing a *consistent* stabilization.

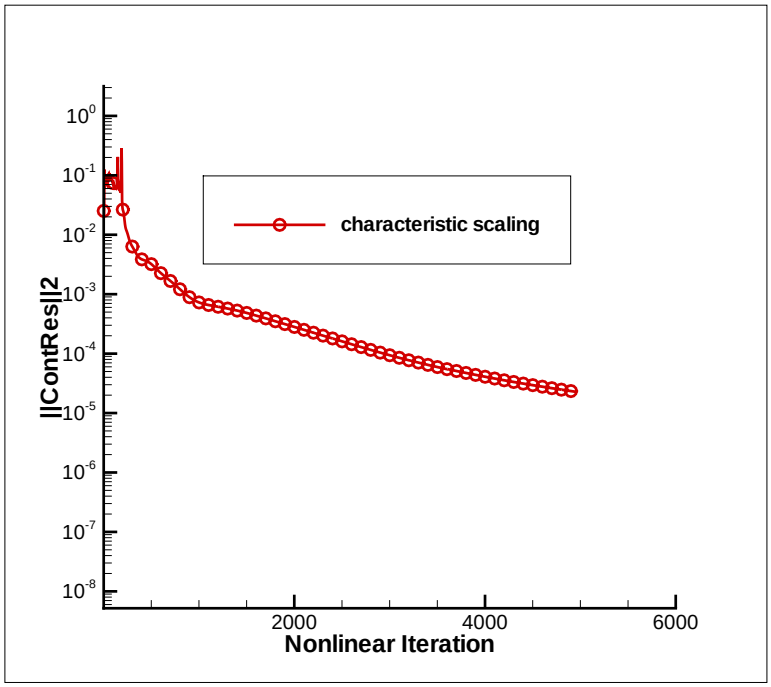

FIGURE 3. Plot of non-linear error norms as a function of non-linear iteration for the characteristic scaling algorithm. In this case, an initial condition of zero is given for all primatives and the steady solution is obtained.

2. Numerical scheme and code base

The newly coupled discretization scheme will use the finite volume technique known as the control volume finite element method of Schneider & Raw (1987). Control volumes (the mesh dual) are constructed about the nodes, as shown in Fig. 4. Each element contains a set of subfaces that define control-volume surfaces. The subfaces consist of line segments (2-D) or surfaces (3-D). The 2-D segments are connected between the element centroid and the edge centroids. The 3-D surfaces are connected between the element centroid, the element face centroids and the edge centroids. Integration points also exist within the subcontrol volume centroids. Such integration points are used for volume integrals such as source terms, the mass matrix, and, if chosen, gradients. For more details of the CVFEM operators, please refer to Domino (2006).

The code base to support fully coupled schemes is the Sandia National Laboratories Advanced Simulation and Computing SIERRA Mechanics which provides internal data structures, scalable parallelism and a common interface for modern linear and non-linear solvers, all within a fully unstructured mesh environment (Edwards & Stewart 2004).

The consolidated Thermal/Fluid code infrastructure, which is built on the SIERRA Mechanics, provides a highly object-oriented framework to implement full analytical sensitivities by the definition of an *expression* class. The *expression* class provides a *sensitivities*() and a *values*() method. Terms within a given partial differential equation are then composed of individual *expressions*. Each *expression* defines a set of *prerequisites*, which are also *expressions*. Therefore, the full hierachy of sensitivities can be automatically generated. However, it is of interest to note that the individual expressions only need to provide derivative information with respect to the terms that

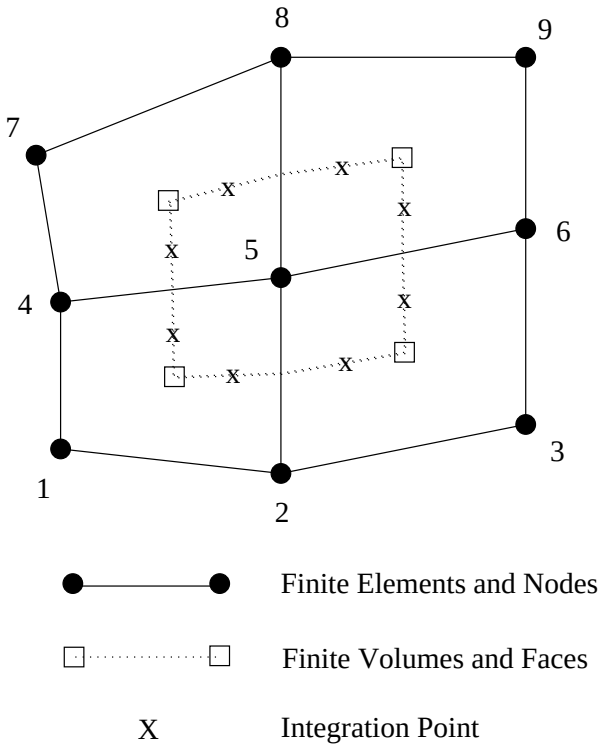

FIGURE 4. A control volume centered about a finite-element node in a collection of 2-D quadrilateral elements.

define the particular expression. As a practical example relevant to this study, consider a functional relationship between density and mixture fraction,

$$\rho(x,y) = \frac{1}{\frac{z(x,y)}{rho^p} + \frac{1-z(x,y)}{rho^s}} \tag{2.1}$$

The density expression lists the degree-of-freedom mixture fraction as a prerequisite. The *values*() method is defined as above while the *sensitivities*() method would be expected to provide $\frac{\partial \rho}{\partial Z}$. This expression could be composed into the mass flux vector and, therefore, contribute sensitivities to the mixture fraction degree-of-freedom from the inclusion of the density *expression* within, for example, the mass flow rate expression, $\rho_j u_j n_j dS$. Finally, other functional expressions for density, e.g., the ideal gas law, exist and can be composed into the mass flux vector without changing the code within the mass flux vector expression.

Additionally, code coupling is naturally supported via surface and volume transfers (currently done via linear interpolation) on potentially non-conformal meshes. In utilizing the SIERRA Mechanics framework, these codes can be coupled to solve a variety of multi-mechanic applications which involve heat transfer between fluid/fluid, fluid/solid and fluid/solid/PMR regions (Domino *et al.* 2007).

During the CTR Summer Program, a fully coupled variable density flow algorithm was implemented. The final mechanics equation set implemented was momentum, continuity

and mixture fraction. Two stabilization orders where coded, again determined by the parameter α as were the two stabilization scaling parameters already discussed in Sec. 1.

3. Methodology for testing

The methodology used to evaluate the accuracy of each proposed scheme will be the method of manufactured solutions (Roache 2002). This powerful verification method provides a high quality metric to determine code correctness and the order of accuracy plot is based on convergence to a known result.

The objective of code verification is to reveal coding mistakes that affect the order of accuracy and to determine if the governing discretized equations are being solved correctly. Quite often, the process of verification reveals algorithmic issues that would otherwise remain unknown. For example, detailed time accuracy verification studies have provided further understanding of stabilized finite volume methods (Domino 2006).

In practice, a variety of comparison techniques exist for verification. For example, benchmark and code-to-code comparison are not considered rigorous due to the errors that exist in other code solutions, such as from discretization and iteration. Analytic solutions and the method of manufactured solutions remain the most powerful methods for code verification, because they provide a means to obtain quantitative error estimations in space and time.

Roache (1998) has made the distinction between code verification and calculation verification, where calculation verification involves grid refinement required for every problem solution to assess the magnitude, not order, of the discretization error. Discretization error, distinguished from modeling and iteration errors, is defined as the difference between the exact solution to the continuum governing equations and the solution to the algebraic systems representation due to discretization of the continuum equations. The order of accuracy can be determined by comparing the discretization error on successively refined grids. Thus, it is desirable to have an exact solution for comparision to determine the discretization errors.

4. Two dimensional steady, uniform, isothermal MMS

The first verification test is a modification of an exact unsteady solution that was first proposed by G. I. Taylor (1923)

$$u(x,y,t) = -u_o \cos(a\pi x)\sin(a\pi y)e^{(-2a^2\pi^2\mu t)} \tag{4.1}$$

$$v(x,y,t) = +v_o \sin(a\pi x)\cos(a\pi y)e^{(-2a^2\pi^2\mu t)} \tag{4.2}$$

$$p(x,y,t) = -\frac{p_o}{4}(\cos(2a\pi x) + \cos(2a\pi y))e^{(-4a^2\pi^2\mu t)}. \tag{4.3}$$

In this solution, the density and viscosity are uniform. Following the assumption of a Newtonian stress tensor, one notes that the convection term cancels the pressure gradient term while the diffusion term cancels the time derivative term (under the assumption that u_o, v_o and p_o and ρ are equal and specified to be unity). This solution can also be modified to support a convecting, decaying Taylor vortex.

Variable	Order of Accuracy					
	L_∞ norm		L_1 norm		L_2 norm	
	decreasing Δx sets $\Rightarrow$		decreasing Δx sets $\Rightarrow$		decreasing Δx sets $\Rightarrow$	
u	1.95	1.99	1.95	1.98	1.96	1.98
v	1.95	1.99	1.95	1.98	1.96	1.98

TABLE 1. Order of accuracy for second-order pressure stabilization with characteristic scaling.

By simply removing the time dependence of the above set of equations, i.e.,

$$u(x,y) = -u_o \cos(a\pi x)\sin(a\pi y) \tag{4.4}$$

$$v(x,y) = +v_o \sin(a\pi x)\cos(a\pi y) \tag{4.5}$$

$$p(x,y) = -\frac{p_o}{4}(\cos(2a\pi x) + \cos(2a\pi y)), \tag{4.6}$$

a formal steady manufactured solution is defined. This solution provides a single source term, as noted above, through the diffusion term since there exists no time term to cancel. The formal steady source terms are as follows:

$$S_u^{mms}(x,y) = -2.0u_o a^2\pi^2\mu\cos(a\pi x)\sin(a\pi y) \tag{4.7}$$

$$S_v^{mms}(x,y) = +2.0u_o a^2\pi^2\mu\sin(a\pi x)\cos(a\pi y) \tag{4.8}$$

$$S_p^{mms}(x,y) = 0.0. \tag{4.9}$$

4.1. *Order of accuracy results*

This solution was tested on grids $25^2, 50^2, 100^2, 200^2$ and 400^2 on a domain of $-0.05 < x < 0.5, -0.05 < y < 0.05$. The values used for density and viscosity are 1.0 and .01 respectively, while the value of the constant a was taken to be 20.

4.1.1. *Second-order stabilization with characteristic scaling*

The simulation was run with the steady fully coupled solver and used a second-order characteristic pressure scaling stabilization ($\alpha = 0$).

Table 1 outline the results for the L_∞, L_1 and L_2 norms for velocities. Results indicate that the velocity field is second-order accurate.

4.1.2. *Fourth-order stabilization with characteristic scaling*

The simulation was run with the steady fully coupled solver and used a fourth-order characteristic pressure scaling stabilization.

Table 2 outlines the results for the L_∞, L_1 and L_2 norms for velocities. Results indicate that the velocity field is second-order accurate.

4.2. *Discussion*

Figures 5 and 6 overview the L_∞, L_1 and L_2 convergence for the second-order and fourth-order stabilization options. Results indicate that the second-order stabilization is less accurate than the fourth-order stabilization method. However, for the 400^2 simulation the number of non-linear solves is only one fewer for the second-order stabilization scheme (21 steps vs. 22 steps). As the characteristic scaling parameter is represented by a nodal assembled quantity, sensitivites to this parameter are not currently included.

Variable	Order of Accuracy					
	L_∞ norm		L_1 norm		L_2 norm	
	decreasing Δx sets $\Rightarrow$		decreasing Δx sets $\Rightarrow$		decreasing Δx sets $\Rightarrow$	
u	2.03	2.02	1.99	2.00	2.03	2.02
v	2.03	2.02	1.99	2.00	2.03	2.02

TABLE 2. Order of accuracy for fourth-order pressure stabilization with characteristic scaling.

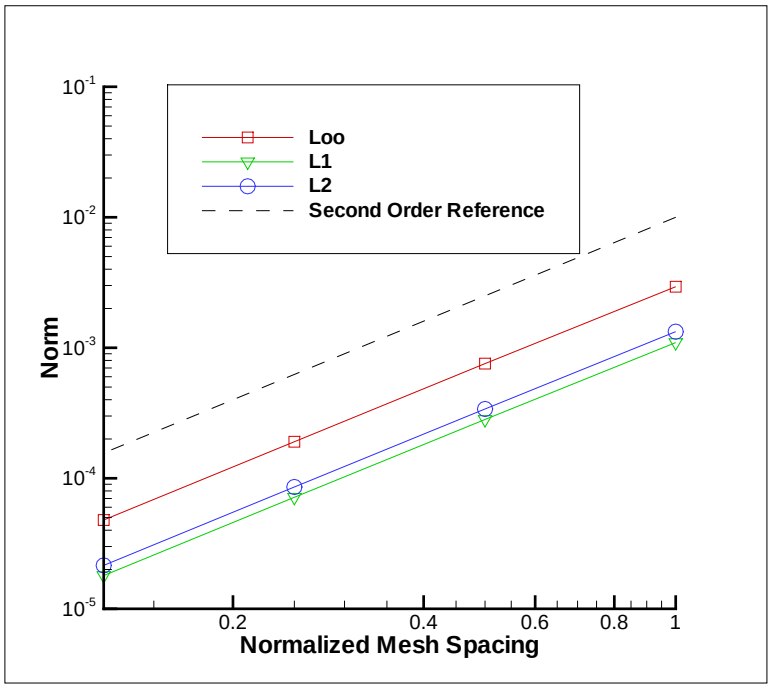

FIGURE 5. Plot of error norms vs. normalized mesh spacing for velocity using the second-order stabilization with characteristic scaling.

Moreover, the assembled pressure gradient is also pre-processed at the top of each non-linear iteration and also does not contribute to the left-hand side of the matrix system. This lack of sensitivity does not seem to affect convergence although work is in progress to include the formal sensitivity in the fully coupled system.

5. Two dimensional steady, uniform, isothermal MMS with passive scalar transport

The second verification test is a modification of the test suite defined by Eqs. 4.5 and 4.6 and only differs by an additional passive scalar transport of a conserved scalar z,

$$z(x, y) = +z_o \cos(a\pi x) \sin(a\pi y). \tag{5.1}$$

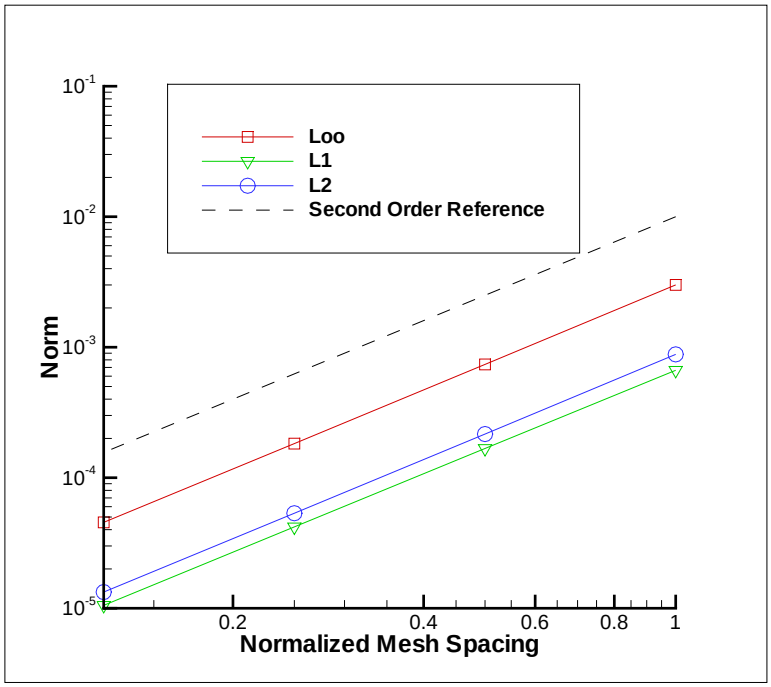

FIGURE 6. Plot of error norms vs. normalized mesh spacing for velocity using the fourth-order stabilization with characteristic scaling.

This test is useful as the current code path differs between vector, i.e., momentum and scalar, i.e., conserved scalar mixture fraction, enthalpy, etc. for the source, advection and diffusion assembly kernels.

The set of source terms for this equation set are as follows:

$$S_u^{mms}(x,y) = -2.0u_o a^2\pi^2\mu\cos(a\pi x)\sin(a\pi y) \tag{5.2}$$

$$S_v^{mms}(x,y) = +2.0u_o a^2\pi^2\mu\sin(a\pi x)\cos(a\pi y) \tag{5.3}$$

$$S_z^{mms}(x,y) = +\frac{1}{Sc}cos(a\pi x)\left(sin(a\pi x)Sc + 2\mu a\pi\sin(a\pi y)\right)a\pi \tag{5.4}$$

$$S_p^{mms}(x,y) = 0.0. \tag{5.5}$$

5.1. *Order of accuracy results*

This solution was tested on grids $100^2, 200^2$ and 400^2 on a domain of $-0.05 < x < 0.05, -0.05 < y < 0.05$. The values used for density and viscosity are 1.0 and .01, respectively, while the value of the constant a was taken to be 20.

Note that since the mixture fraction is a passive scalar and does not couple to the momentum field, the order of convergence was verified to be the same as the first verification result. Given this, only the fourth-order smoothing scheme for the $100^2, 200^2, 400^2$ refinement set is presented.

5.1.1. *Fourth-order stabilization with characteristic scaling*

The simulation was run with the steady fully coupled solver and used a fourth-order characteristic pressure scaling stabilization.

Variable	Order of Accuracy		
	L_∞ norm fine mesh set	L_1 norm fine mesh set	L_2 norm fine mesh set
u	2.02	2.00	2.02
v	2.02	2.00	2.02
z	2.00	2.00	2.00

TABLE 3. Order of accuracy for fourth-order pressure stabilization with characteristic scaling with passive scalar transport.

Table 3 outlines the results for the L_∞, L_1 and L_2 norms for velocity and mixture fraction. Results indicate that the velocity and mixture fraction field are second-order accurate.

6. Two dimensional steady, non-uniform, isothermal MMS with scalar transport

The third and final verification test presented in this initial work is a modification of the test suite defined by Eqs. 5.3 and 5.5 that now includes variable density with the scalar transport of a conserved scalar, z (now chosen to be bounded between zero and unity),

$$u(x,y,t) = -u_o \cos(a\pi x)\sin(a\pi y) \tag{6.1}$$

$$v(x,y,t) = +v_o \sin(a\pi x)\cos(a\pi y) \tag{6.2}$$

$$p(x,y,t) = -\frac{p_o}{4}(\cos(2a\pi x) + \cos(2a\pi y)) \tag{6.3}$$

$$z(x,y) = +z_o \cos(\hat{a}\pi x)\cos(\hat{a}\pi y) \tag{6.4}$$

Moreover, the equation of state for density is based on the density mixture fraction expression again provided by Eq. (2.1),

$$\rho(x,y) = \frac{1}{\frac{z(x,y)}{rho^p} + \frac{1-z(x,y)}{rho^s}} \tag{6.5}$$

The set of source terms for this equation are too complex to outline here; however, it is noted that the continuity equation now includes a right hand source term. Also, the equation set now includes a non-divergence-free velocity which augments the standard Newtonian viscous stress tensor and is given by $-\frac{2}{3}\mu\frac{\partial u_j}{\partial x_j}\delta_{ij}$.

6.1. *Order of accuracy results*

This solution was tested on grids $100^2, 200^2$ and 400^2 on a domain of $-0.05 < x < 0.05, -0.05 < y < 0.05$ and $-0.0375 < x < 0.0625, -0.0375 < y < 0.0625$. Values of ρ^p and ρ^s are 1.0 and 2.0 respectively, while values of a and $\hat{a}$ are 20 and 10. It is noted that the second mesh domain provides a normal pressure derivative to be non-zero at all exposed surfaces.

Figure 7 represents an elevated surface for the x-component of velocity, colored by the x-component of velocity while Fig. 8 represents an elevated surface for the mixture fraction colored by density.

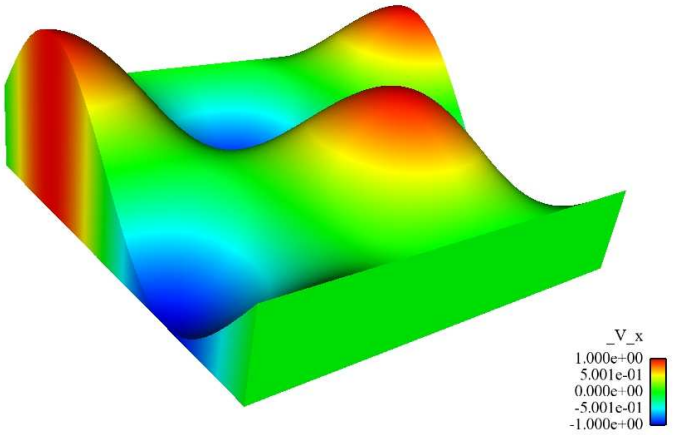

FIGURE 7. Elevated surface plot of x-component of velocity colored by x-component of velocity.

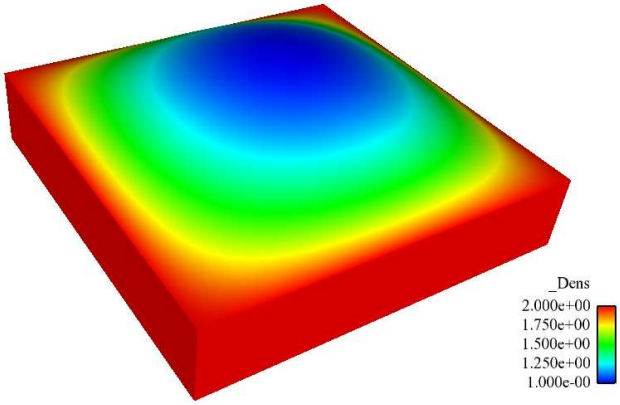

FIGURE 8. Elevated surface plot of mixture fraction colored by density.

6.1.1. *Second-order stabilization with characteristic scaling,* $\frac{\partial p}{\partial n} = 0$

The simulation was run with the steady solver and used a second-order characteristic pressure scaling stabilization.

Table 4 outlines the results for the L_∞, L_1 and L_2 norms for velocity and mixture fraction. Results indicate that the velocity and mixture fraction field are again second-order accurate.

6.1.2. *Second-order stabilization with characteristic scaling,* $\frac{\partial p}{\partial n}! = 0$

The simulation was run with the steady solver and used a second-order characteristic pressure scaling stabilization.

Table 5 outlines the results for the L_∞, L_1 and L_2 norms for velocity and mixture fraction. Results indicate that the velocity and mixture fraction field are again second-order accurate.

Variable	Order of Accuracy		
	L_∞ norm	L_1 norm	L_2 norm
	fine mesh set	fine mesh set	fine mesh set
u	2.01	1.99	2.00
v	2.01	1.99	2.00
z	2.00	1.99	2.00

TABLE 4. Order of accuracy for variable density second-order pressure stabilization with characteristic scaling with scalar transport, $\frac{\partial p}{\partial n} = 0$.

Variable	Order of Accuracy		
	L_∞ norm	L_1 norm	L_2 norm
	fine mesh set	fine mesh set	fine mesh set
u	1.99	1.97	1.98
v	1.99	1.97	1.98
z	2.05	2.00	2.02

TABLE 5. Order of accuracy for variable density second-order pressure stabilization with characteristic scaling with scalar transport, $\frac{\partial p}{\partial n}! = 0$.

Variable	Order of Accuracy		
	L_∞ norm	L_1 norm	L_2 norm
	fine mesh set	fine mesh set	fine mesh set
u	2.00	2.00	2.01
v	2.00	2.00	2.01
z	2.00	2.00	2.00

TABLE 6. Order of accuracy for variable density fourth-order pressure stabilization with characteristic scaling with scalar transport, $\frac{\partial p}{\partial n} = 0$.

6.1.3. *Fourth-order stabilization with characteristic scaling,* $\frac{\partial p}{\partial n} = 0$

The simulation was run with the steady fully coupled solver and used a fourth-order characteristic pressure scaling stabilization.

Table 6 outlines the results for the L_∞, L_1 and L_2 norms for velocity and mixture fraction. Results indicate that the velocity and mixture fraction field are again second-order accurate.

6.1.4. *Fourth-order stabilization with characteristic scaling,* $\frac{\partial p}{\partial n}! = 0$

The simulation was run with the steady solver and used a fourth-order characteristic pressure scaling stabilization.

Table 7 outlines the results for the L_∞, L_1 and L_2 norms for velocity and mixture fraction. Results indicate that the velocity and mixture fraction field are again second-order accurate.

Variable	Order of Accuracy		
	L_∞ norm	L_1 norm	L_2 norm
	fine mesh set	fine mesh set	fine mesh set
u	2.05	2.00	2.02
v	2.05	2.00	2.02
z	1.99	1.99	1.99

TABLE 7. Order of accuracy for variable density fourth-order pressure stabilization with characteristic scaling with scalar transport, $\frac{\partial p}{\partial n}! = 0$.

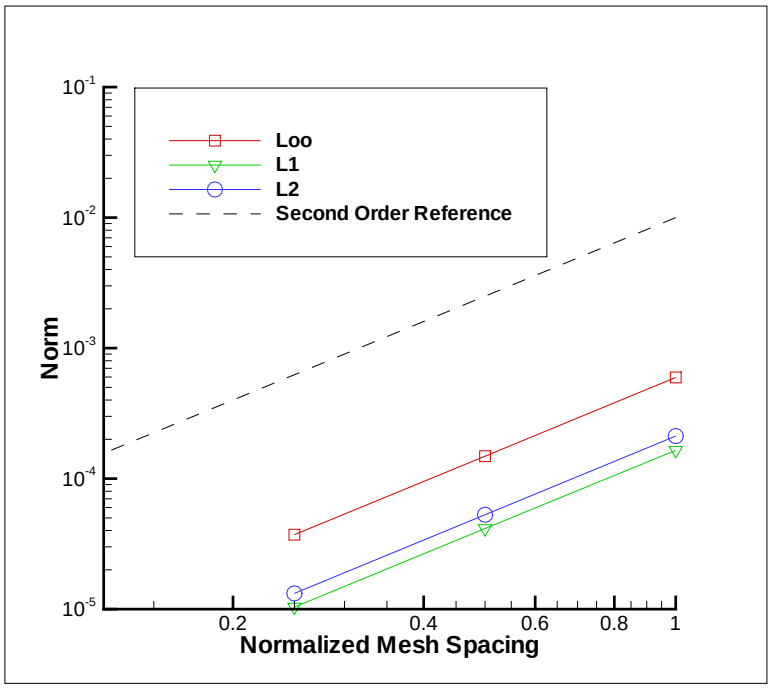

FIGURE 9. Plot of error norms vs. normalized mesh spacing for velocity using the fourth-order stabilization with characteristic scaling (variable density).

6.2. *Discussion*

Figure 9 shows the convergence plot for the velocity while Fig. 10 outlines the convergence plot for mixture fraction each in the case for fourth order smoothing with characteristic scaling with the normal pressure derivative equal to zero.

7. Future work

Due to time constraints, the author is unable to provide formal manufactured solution verification results for transient flows. However, during the Summer Program, a convecting, decaying Taylor vortex problem was run with both scaling parameters in the context of the fully coupled scheme using a first-order backward Euler time integrator. A second-order time integration scheme is currently being implemented and was not available for

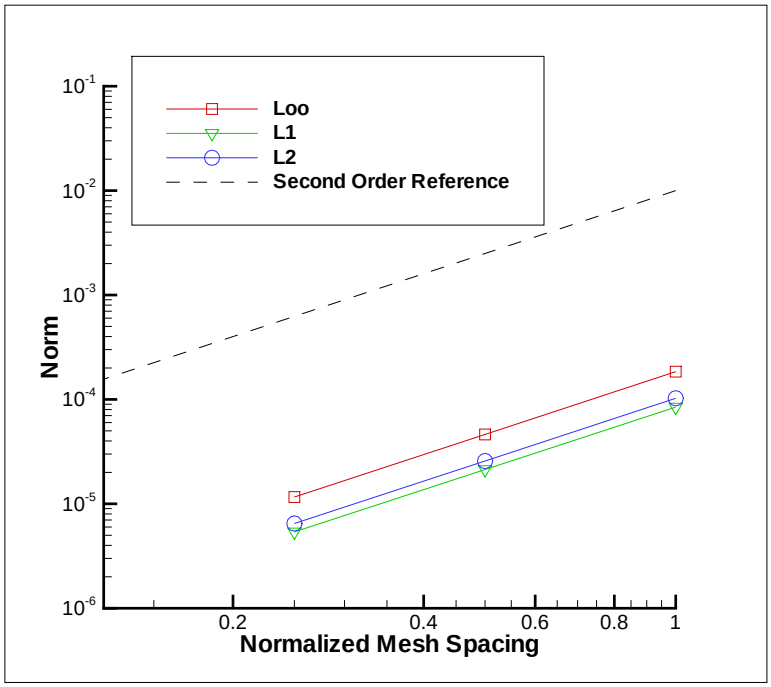

FIGURE 10. Plot of error norms vs. normalized mesh spacing for mixture fraction using the fourth-order stabilization with characteristic scaling (variable density).

this study. Moreover, a transient manufactured solution with variable density has been proposed, which is again based on the exact solution of Taylor, and is given by:

$$u(x,y) = -u_o \cos(a\pi x)\sin(a\pi y)\sin(\omega t) \tag{7.1}$$

$$v(x,y) = +v_o \sin(a\pi x)\cos(a\pi y)\sin(\omega t) \tag{7.2}$$

$$p(x,y) = -\frac{p_o}{4}(\cos(2a\pi x) + \cos(2a\pi y))\sin^2(\omega t) \tag{7.3}$$

$$z(x,y) = +z_o \cos(\hat{a}\pi x)\cos(\hat{a}\pi y)\sin(\omega t). \tag{7.4}$$

Again, the functional form of density given by q. (2.1).

8. Conclusions

An equal-order fully coupled scheme, with full analytical Jacobians, has been implemented in the Sierra Mechanics code base. This stabilized, fully coupled scheme has been verified to be spatially second-order accurate using a set of uniform and non-uniform (variable density) manufactured solutions. Two different stabilization orders have been implemented, each of which are very robust and convergent.

This study represents a high quality verification-based methodology that is presented for evaluating order of convergence for any low-Mach-number algorithms.

Acknowledgments

Sandia is a multiprogram laboratory operated by Sandia Corporation, a Lockheed Martin Company, for the United States Department of Energy under Contract DE-AC04-94AL850000.

The author would like to thank the CTR host, Dr. Frank Ham, for his time during the Summer Program.

REFERENCES

Almgren, A. S., Bell, J. B. & Crutchfield, W.Y. 2000 Approximate projection methods: part I. inviscid analysis. *SIAM J. Sci. Comp.*, **22**, 1139–1159.

Bochev, P., Gunsburger, M. & Lehoucq, R. 2007 On stabilized finite element methods for the Stokes problem in the small time step limit. *.Int. J. Num. Meth. Fluids.*, **53(4)**, 573–597.

Codina, R. & Badia, S. 2005 On some pressure segregation methods of fractional-step type for the finite element approximation of incompressible flow problems. *Comp. Methods. Appl. Mech. Engr.*, in press.

Domino, S. P. 2006 Toward verification of formal time accuracy for a family of approximate projection methods using the method of manufactured solutions. *Proceedings of the 2006 Summer Program, Center for Turbulence Research*, **11**, 163–177.

Domino, S. P., Wagner, G. J, Luketa-Hanlin, A., Black, A. & Sutherland, J. 2007 Verification for multi-mechanics applications. *Paper AIAA2007-1933*, 48th AIAA/ASME/ASCE/AHS/ASC Structures, Structural Dynamics, and Materials Conference, Honolulu, HI.

Edwards, H. C., & Stewart, J. R. 2004 A framework approach for developing parallel adaptive multiphysics applications. *Finite Elements in Analysis Design*, **40(12)**, 1599–1617.

Ghia, U., Ghia, K. N. & Shinn, C. T. 1983 High-RE solutions for incompressible flow using the Navier-Stokes equations and a multigrid method. *J. Comp. Phys.*, **48**, 387–411.

Roache, P. J. 1998 Verification of codes and calculations. *AIAA J.*, **36(5)** 696–702.

Roache, P. J. 2002 Code verification by the method of manufactured solutions. *J. Fluids Engr.*, **124(1)** 4–10.

Schneider, G. E. & Raw M. J. 1987 Control Volume Finite-Element Method for Heat Transfer and Fluid Flow Using Colocated Variables–1. Computational Procedure. *Num. Heat Trans.*, **11** 363–390.

Taylor, G. I. 1923 On the decay of vortices in a viscous fluid *Phil. Mag.*, **46** 671–674.